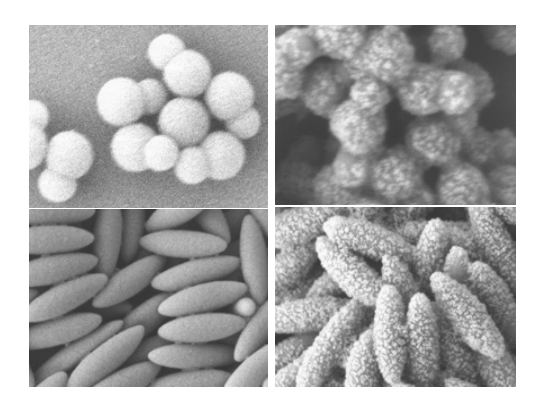
Graphical Abstract

Magnetic properties, responsiveness, and stability of paramagnetic dumbbell and ellipsoid colloids Hojin Kim,Eric M. Furst



Magnetic properties, responsiveness, and stability of paramagnetic dumbbell and ellipsoid colloids

Hojin Kim^a, Eric M. Furst^a

^aDepartment of Chemical and Biomolecular Engineering, Allan P. Colburn Laboratory, University of Delaware, Newark, DE 19716, United States

ARTICLE INFO

Keywords: magnetic particle layer-by-layer anisotropic particle directed self-assembly

ABSTRACT

A layer-by-layer method is used to synthesize paramagnetic metal/polymer multi-layered colloidal particles. By taking advantage of recent advances in the synthesis of polymer colloids with various shapes and layer-by-layer assembly, superparamagnetic dumbbell colloids are fabricated with different aspect ratios and asymmetries between lobes. We characterize the surface coverage of magnetic nanoparticles on the anisotropic host particles and the magnetic response of the particles by magnetometry. The synthesized particles are colloidally stable, but in a magnetic field, form persistent microstructures through induced interactions. These column-like microstructures are reversible and readily disperse by Brownian motion. The magnetic nanoparticle concentration during synthesis provides a means to control the magnetic response of the composite nanoparticle. The method is extended to prolate ellipsoid nanoparticles with aspect ratios between 3.4 and 4.2.

1. Introduction

The directed self-assembly of colloids and nanoparticles can be harnessed to fabricate nanostructured materials with photonic and phononic properties that are programmed by particle shape and interactions.[1, 2, 3, 4, 5, 6] Directing external electric, magnetic, or deformation (e.g. shear or extensional) fields are necessary to circumvent kinetic bottlenecks to self-assembly, especially for anisotropic particles, like ellipsoids and dumbbells.[3, 7, 8, 9] But a current challenge in the directed-self assembly of colloids by electric or magnetic fields lies in the decrease of the field-induced alignment and interactions between particles as their size decreases, since the particle polarization scales with the particle volume.[10] While one can use higher field strengths, ultimately this strategy is limited—in electric fields by the dielectric breakdown and hydrolysis at the electrodes[11, 12] and in magnetic fields by the saturation magnetization of the particles. These limitations point to an opportunity to develop synthesis strategies for highly polarizable anisotropic magnetic colloids for self-assembly applications.

Recent developments in synthesis methods have given rise to magnetic colloids with a variety of chemical compositions and shapes, but few of these methods produce particles with a paramagnetic response that has been useful for assembly in toggled external fields.[13, 14] Ferromagnetic colloids have been synthesized by Ge *et al.*, who created anisotropic magnetite (Fe₃O₄)-silica (SiO₂)-polystyrene (PS) composite ellipsoids and doublets by seeded emulsion polymerization.[15] Based on a spherical Fe₃O₄/SiO₂ core/shell NPs as a seed, the shape of magnetite/silica composite particles are changed into spherical, ellipsoidal, and asymmetric doublet particles by polymerizing PS around the seeds. Ding and coworkers presented a synthesis method for ferromagnetic ellipsoids by coating silica shell atop of hematite spindles.[3, 4] The as-

E-mail: furst@udel.edu (E.M. Furst)
ORCID(s):

pect ratio of ellipsoids are tuned by either using different aspect ratio of the spindles or varying the concentration of tetraethoxysilane (TEOS). In contrast to these methods, Senyuk et al. reported the synthesis of magneticallyresponsive dumbbell-shaped PS particles after the shape is formed without any chemical reactions.[16] PS anisotropic particles with an order of few micrometers in size were swollen by CoFe₂O₄ NPs dispersed in toluene to incorporate magnetic NPs into the PS particles. However, these methods require an anisotropic core precursor, the anisotropic growth of polymers, or a seed polymer that can be swollen by a medium containing magnetic particles. Other synthesis strategies include mechanically stretching ferromagnetic latex particles, but the remnant magnetization of the particles causes aggregation that prevents suspensions from reaching an equilibrium structure.[17]

Instead, one can make use of the wide range of particle shapes fabricated by recent advances in polymer colloid synthesis, [18, 19, 20, 21] by making composite particles of magnetic and non-magnetic colloids. Caruso et al. first presented such a method using a layer-by-layer (LbL) strategy to synthesize PS/magnetite NP core/shell spherical beads. The sequential adsorption of oppositely charged polyelectrolytes and charged magnetic NPs coats the PS spheres with magnetite NPs. Due to the magnetic moments of magnetite NPs, these particles align into chains in the presence of external magnetic field.[22] This method was further investigated to fabricate superparamagnetic particles and to form permanent chains.[23] Besides the electrostatic interaction, non-electrostatic forces have been used for functionalizing anisotropic dimers with metallic nanoparticles.[24] Because maghemite $(\gamma - \text{Fe}_2 \text{O}_3)$ NPs are superparamagnetic, PS/maghemite core/shell particles have no residual magnetization. The LbL method has also been applied to anisotropic platelets[1, 25] and carbon nanotubes[26] to create magnetic responsive composite materials.

In this article we fabricate magnetically-responsive anisotropic nanoparticles with dumbbell and ellipsoidal

shapes using the LbL adsorption method. By taking advantage of both the well-developed LbL method and scalable synthesis of anisotropic polymer colloids, we transform non-magnetic polymer nanoparticles with various shapes to particles that exhibit strong magnetophoresis and self-assembly in magnetic fields. We tune the magnetic properties of the particles by varying the amount of magnetic NPs. The colloids show similar magnetic response and assembly behavior with commercial paramagnetic beads under magnetic fields and can be synthesized in quantities sufficient to study their bulk assembly.

2. Materials and Methods

2.1. Materials

Styrene (≥ 99%), sodium 4-vinylbenzenesulfonate 90%), 3-(trimethoxysilyl)propyl acrylate $(NaVBS, \geq$ (TMSPA, 92%), 2,2'-azobis (2-methylpropionitrile) (AIBN, 98%), potassium persulfate (KPS, \geq 99.0%), poly (diallyl dimethyl ammonium chloride) (PDADMAC, $M_W < 100,000, 35$ wt % in water), polystyrene sulfonate (PSS, M_W =70,000), iron(III) chloride hexahydrate (Fe(III)Cl₃·6H₂O, 97%), and poly (vinyl alcohol) (PVA, M_W =146,000-186,000, > 99%) are purchased from Sigma-Aldrich. Sodium chloride, ammonium hydroxide (NH₄OH, 28.0 - 30.0 w/w %), isopropyl alcohol (IPA, \geq 99.5%), and methanol (99.9%) are purchased from Fisher Scientific. Citric acid monohydrate (99.5%) and iron(II) chloride tetrahydrate (Fe(II)Cl₂·4H₂O, \geq 99%) are purchased from Acros Organics. The chemicals are used as received. The DI water used is filtered with a Millipore Direct-Q 5 ultra purification system (resistivity $\rho > 18.2 \text{ M}\Omega \cdot \text{cm}$).

2.2. Synthesis of Dumbbell-Shaped Particles

The PS NPs are synthesized by the surfactant-free emulsion polymerization and have charged functional groups at the surface. [27, 28] The surface charges create a repulsive double layer interaction between the particles and it results in good dispersion quality and colloidal stability. The LbL strategy here uses the surface charge to interact electrostatically with oppositely charged species, such as polyelectrolytes or charged metal NPs. As a result of this interaction, multilayers of polyelectrolytes can be adsorbed on the surface so that the surface charge and the chemical composition can be modified. In addition to the electrostatic interaction, the hydrophobic interactions also contribute to the adsorption of the polyelectrolytes. [29] Here, the LbL method is used to coat the superparamagnetic NPs onto the anisotropic dumbbell-shaped (DB) and ellipsoidal polymer particles.

We illustrate the LbL strategy for coating the magnetite NPs onto the surface of the anisotropic colloidal particles in Figure 1. The DB NPs used for this study consist of two different chemical compositions. The seed particle side is functionalized by the TMSPA which contains acrylate groups. The second lobe does not have TMSPA. The polyelectrolytes are next adsorbed onto the surfaces of the DB NPs.[30, 29] The cationic polyelectrolyte, PDADMAC is first adsorbed.

The adsorption of the PDADMAC layer transforms the surface into a cationic surface, allowing the subsequent adsorption of a polyelectrolyte multilayer. The anionic polyelectrolyte PSS is adsorbed next. Consequently, a series of PDADMAC, PSS, and PDADMAC adsorption steps is performed. The PDADMAC-terminated DB NPs obtain cationic surface charges and therefore, the citrate ion-coated magnetite NPs with negative charges can coat the DB NPs. An excess amount of the magnetite NPs is used, and the nonadsorbed magnetite NPs and the nonmagnetic dumbbells are removed from the supernatant when the fabricated magnetic dumbbells are decanted by an external magnet.

The submicron size dumbbell-shaped particles are prepared via the two-step seeded emulsion polymerization as described elsewhere.[31] First, the polystyrene (PS) seed particles with a diameter d = 150 nm are synthesized.[32] A mixture of 25 ml styrene and 0.2 g NaVBS dissolved in 150 ml of water and methanol mixture (3:1 volume ratio) solution is polymerized with 0.11 g of KPS at 65 °C. For the PS/poly (St-co-TMSPA) core/shell particles, the synthesized seed PS spheres (5 v/v %) suspended in water are then swollen in the presence of 0.3 mg/ml AIBN initiator in a styrene (6 v/v %) and TMSPA (0.6 v/v %) mixture for 30 min at room temperature. The swollen particles are heated to 70 °C and the polymerization is continued for 8 hours or more. Next, the synthesized core/shell particles (4 v/v %) are swollen again by styrene (4 v/v %) for 30 min under gentle vortexing and are polymerized at 70 °C for 8 hours. Finally, after quenching the polymerization, the particles are washed by centrifugation and the supernatant is replaced with high-purity water at least three times. The aspect ratio is controlled by the amount of styrene used for swelling the core/shell particle; lower styrene amounts result in smaller protrusion sizes.

2.3. Synthesis of Ellipsoidal Particles

The PS ellipsoid particles are synthesized by mechanically stretching the PS seed particles with a diameter of d =400 nm (Invitrogen, Eugene, OR, cat#C37238). The details of the synthesis method are described elsewhere.[33, 34] Briefly, the seed PS spherical particles dispersed in the aqueous PVA solution are spread in a dish and dried to a thin film. The thin film is heated in a silicon oil bath for 5 min at 145 °C, which is above the glass transition temperature of PS particles, and stretched. Then, the film is cooled down to room temperature and washed with IPA at least 5 times to remove silicon oil. The embedded particles in the film are recovered in a mixture of water and IPA (7:3 v/v ratio). The particles are then washed by stirring for 12 hours while being heated at 75 °C. The suspensions are centrifuged and resuspended in water/IPA solution and these steps are repeated at least three times. Finally, the particles are suspended in water.

2.4. LBL Adsorption of Dumbbell-Shaped Particles

The polyelectrolytes are adsorbed onto the surface of the anisotropic particles using the LbL method to alternate the

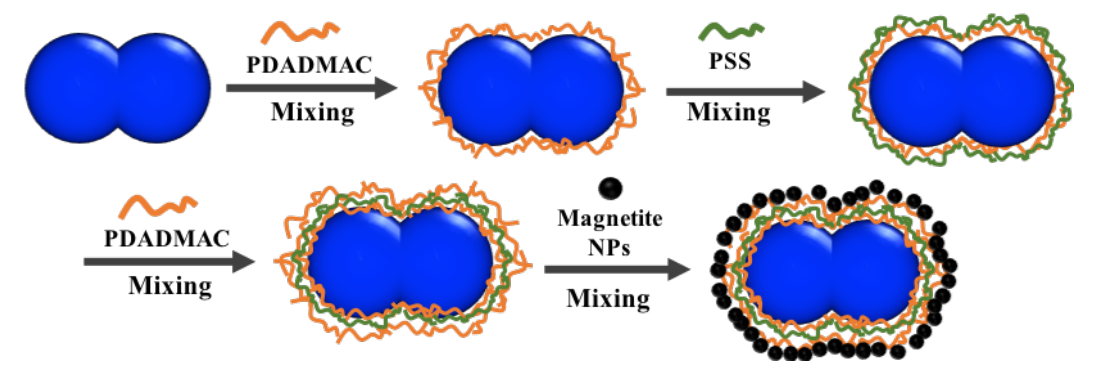


Figure 1: The layer-by-layer method for the superparamagnetic metal/polymer multi-layered nanoparticles. This method is illustrated for the dumbbell-shaped NPs. The PDADMAC (cationic) and PSS (anionic) polyelectrolytes are assigned with orange and green, respectively. The magnetite NPs are marked with black dots.

colloidal particle surface charge. 0.5 ml of the suspension containing the DB (or ellipsoidal) particles (0.5 wt %) is mixed with 0.5 ml of PDADMAC solution (20 mg/ml in 0.5 M NaCl aqueous solution) and the mixture is vortexed for 30 min to reach a saturation concentration. After mixing, the excess PDADMAC in solution is removed by repeated centrifugation (6,000 rpm for 15 min) and the supernatant medium is replaced with water three times. The first adsorption results in an excess of polyelectrolyte.[35] The adsorption of subsequent PSS and PDADMAC layers should reduce the amount of polyelectrolyte desorption while the magnetite NPs are coated. This step improves the coating quality of magnetite NPs and the colloidal stability of the composite magnetic particle.

2.5. Synthesis of Iron Oxide Nanoparticles

The superparamagnetic magnetite NPs with a diameter $d=8.0\pm1.3$ nm are synthesized by the co-precipitation method and the synthesized particles are stabilized by coating citrate ions as described elsewhere.[36] 0.48 g of Fe(II)Cl₂·4H₂O and 1.31 g of Fe(III)Cl₃·6H₂O are mixed in 22 ml of water under nitrogen gas with vigorous magnetic stirring (1,100 rpm). The solution is heated to 60 °C for 30 min and 2.8 ml of NH₄OH is slowly added with a rate of 23 μ l/s. After the addition, 0.56 g of citric acid monohydrate dissolved in 1 ml of water is added into the solution and the temperature is heated to 95 °C and kept for 90 min. The synthesized NPs are washed by decanting iron oxide magnetically and the medium is replaced with water twice.

2.6. Magnetite Nanoparticles Coating on Anisotropic Nanoparticles

The anisotropic colloidal particles with cationic surface charges are electrostatically coated by the magnetite NPs (negatively charged surface).[22, 23] 0.2 ml of 0.5 wt % of the anisotropic particle dispersed in water is mixed with 0.09 ml of 1.3 wt % (0.4 wt % in total) and 0.12 ml of 1.3 wt % (0.5 wt % in total) magnetite NP. The mixture is vortexed for 30 min. The excess amount of the nonadsorbed magnetite NPs and the uncoated anisotropic particles are decanted magnetically and washed with water three times.

2.7. Analysis and Characterization Methods

The magnetization curves are measured using the vibrating sample magnetometer (VSM, VersaLab). The applied field is cycled from 10 kOe to -10 kOe with a 50 Oe/s step rate at 300 K. To further analyze the remnant magnetization at zero magnetic field, magnetic properties are again measured by cycling the applied field from 300 Oe to -300 Oe with a 10 Oe/s step rate at the same temperature.

An optical microscopy (Microscope Axio Observer Ai Zeiss AXIO) is used with a 40x objective and the images are recorded with a digital SLR camera (Canon-EOS Digital Rebel T2i). Scanning electron microscopy images are taken using a JEOL JSM-7400F with 3 keV accelerating voltage. A thin layer of gold and palladium are sputter-coated to the sample before imaging. Transmission electron microscopy images are collected using a JEOL JEM-3000 operating at 300 keV and a FEI Talos F200C microscope operating at 200 kV. The samples are prepared on a carbon-coated copper grid with 300 mesh (Electron Microscopy Sciences).

3. Results and Discussion

3.1. Structure of Anisotropic Magnetic Nanoparticles

The nanostructure of the DB/magnetite NPs are shown in Figure 2. Figure 2a is a transmission electron microscope (TEM) image of magnetite NPs with diameter, $d = 8.0 \pm 1.3$ nm. The mean diameter of magnetite NPs is estimated based on a log-normal model. Figure 2b is the histogram of magnetite NPs with the bin-width, W, decided by the Sturges' rule using the relation $W = (d_{\text{max}} - d_{\text{min}})/k$, where the number of bins $k = 1 + \log_2 N$ with sample size N and the maximum d_{max} and minimum d_{min} size of magnetite NPs.[37] This size distribution is in a good agreement with a log-normal function (a red solid line). Asymmetric and symmetric DB NPs, DB1 (Figure 2c) and DB2 (Figure 2d), respectively, have average diameters of smaller (d_1) and bigger (d_2) lobes and an average particle length (L); for DB1 $d_1 = 146 \pm 1$ nm, $d_2 = 146 \pm 1$ nm, and $L = 294 \pm 2$ nm and for DB2, $d_1 = 196 \pm 2$ nm, $d_2 = 221 \pm 2$ nm, and $L = 362 \pm 2$ nm.

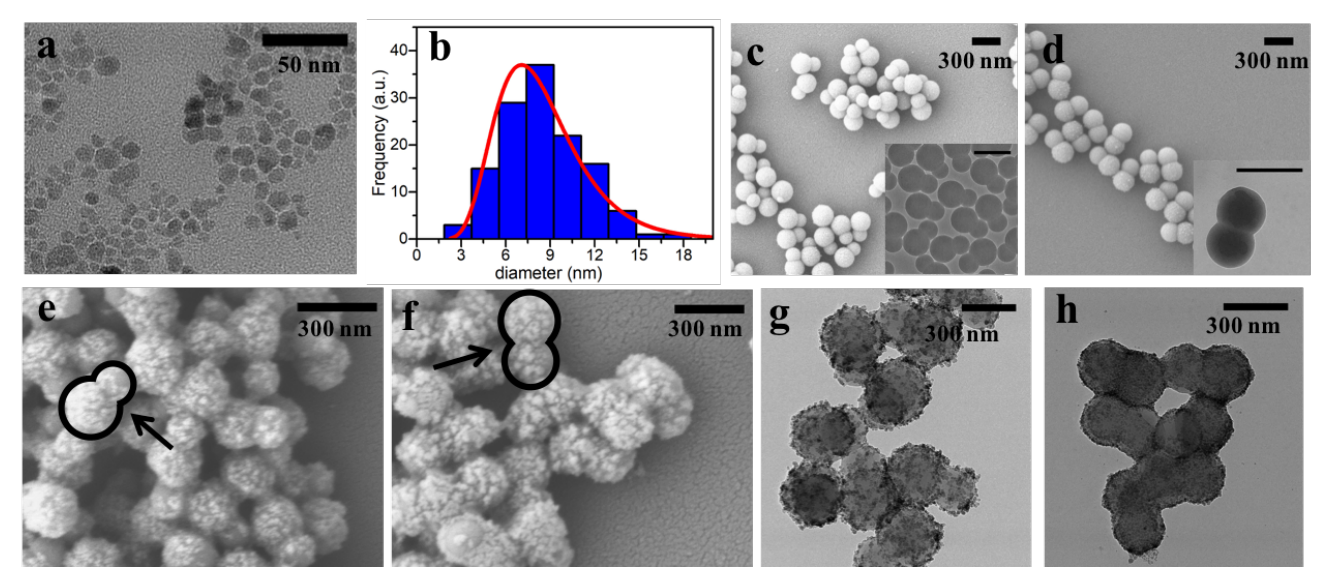


Figure 2: a Transmission electron microscopy (TEM) image of magnetite NPs particles with an average diameter $d=8.0\pm1.3$ nm. b The histogram of magnetite particle size distribution and the the corresponding log-normal function (red solid line). Scanning electron microscope (SEM) images of c DB1and d DB2 particles before the layer-by-layer adsorption of magnetite NPs. e and f show SEM images of DB1 and DB2 particles coated by magnetite nanoparticles, respectively. g and h show corresponding TEM images of superparamagnetic DB1 and DB2 NPs. Arrows and solid lines in e and f highlight magnetite coated DB particles. Scalebars of the insets in c and d: 300 nm.

DB1 and DB2 NPs coated by the magnetite particles are shown in Figure 2e and 2f, respectively. The surface of the original DB NPs is smooth and uniform as shown by TEM images of particles in the inset of Figure 2c and 2d. After coating, the magnetite NPs are distributed on the surface of DB NPs and make the surface rough, regardless of their anisotropy or symmetry. TEM images of the magnetite NP-coated DB NPs (shown in Figure 2g and 2h) verifies that the adsorption is uniform and that there is no aggregation or excessive amount of adsorbed magnetite NPs on the DB NPs surfaces. Using the LbL method allows for a uniform coating of metal NPs without chemically functionalizing the DB NPs.

At this stage in the magnetite NPs coating, the stability of the colloidal magnetite NPs plays a crucial role in forming a uniform surface coating. To test the effect of magnetite NP stability, DB NPs are coated by two different magnetite NPs that are stable and unstable in water. The quality of surface adsorption is compared using scanning electron microscopy. The stability of magnetite NPs is controlled by changing the addition rate of base while the magnetite NPs are precipitated.[38] Unlike the stable magnetic NPs shown earlier in Figures 2d and 2e, the unstable magnetite NPs do not coat the DB NPs, but rather create aggregates (Figure S1). This can be attributed to short-range interactions between the magnetite NPs, which is stronger than with the multilayer-adsorbed polymer DB NP surfaces.[30]

Ellipsoidal PS NPs shown in Figure 3a and 3b are studied next to verify that the LbL method is versatile and can be applied to other seed particle shapes. Two ellipsoids with different aspect ratios L/d=3.4 (EP3.4) and 4.2 (EP4.2), where L and d refer to particle length and diameter, respec-

tively, are used for magnetite NP coating. The seed particles for ellipsoidal particle synthesis are negatively charged from sulfate and carboxyl groups. The ellipsoids are fabricated by mechanical stretching above their glass transition temperature (details in Methods)[33]. The LbL adsorption between the ellipsoid surface and polyelectrolytes is mainly due to electrostatic interactions. The same LbL adsorption of polyelectrolytes and magnetite NPs produces an ellipsoidal PS/magnetite (EP/magnetite) core/shell structure for which magnetite NPs are well-adsorbed onto the surfaces of ellipsoids for EP3.4 (Figure 3c) and EP4.2 (Figure 3d) particles. This corroborates the concept that the LbL adsorption of polyelectrolytes and magnetite NPs can be widely applied into other particle shapes with various curvatures to make magnetic responsive anisotropic NPs.

As SEM micrographs of magnetic ellipsoids show (Figure 3c and 3d), the magnetite NPs are distributed uniformly along the surface of the non-magnetic NPs, but are not closely-packed. The distribution and total magnetite content is important to know in order to tune the magnetic interactions between composite particles, as we discuss in the next section. We examined the intensity of scanning electron micrographs along the composite nanoparticle surfaces (e.g., Figure 3c). An analysis of the intensity distribution peaks from the plot (Figure 3) provides a measure of the size and distribution of magnetite NPs on the surface. The full width at half maximum (FWHM) values are determined by fitting the intensity distribution peaks with a series of Gaussian distributions. These peaks indicate that nanoparticle clusters of size scale approximately 33.5 ± 4.8 nm in diameter, corresponding to approximately four magnetite NPs, are arranged on the surface with 17.0 ± 4.4 nm average edge-to-edge dis-

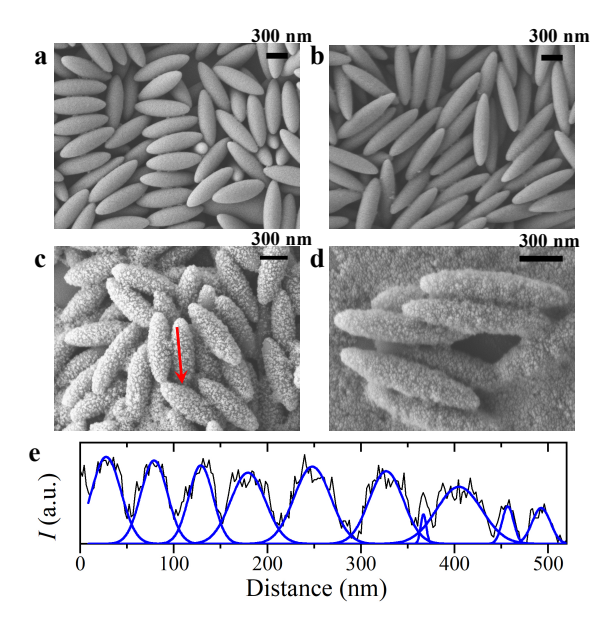


Figure 3: Scanning electron microscopy (SEM) images of ellipsoidal PS particles with aspect ratio a L/d=3.4 (EP3.4) and b 4.2 (EP4.2) before magnetite nanoparticle coating. c and d are SEM images of EP3.4/magnetite and EP4.2/magnetite multi-layered particles, respectively. Scale bars are 300 nm. e Estimation of brightness intensity along the line described in c shows peaks which indicate coated magnetite nanoparticles. Blue lines indicate Gaussian fitting of intensity plot for full width at half maximum, which gives magnetite nanoparticle size distributions.

tance between clusters.

3.2. Magnetic Properties of the Anisotropic Magnetic Nanoparticles

Composite nanoparticles synthesized by the LBL process retain the superparamagnetic properties of the magnetite NPs. The magnetic properties of the multilayer DB/magnetite NPs and the pure magnetite NPs are measured with a vibrating sample magnetometer (VSM). We plot the magnetization curves in Figure 4 for the magnetite NPs and DB/magnetite multi-layered NPs as the magnetic moment, M (Am²/kg), versus the applied magnetic field, H (kA/m) at a temperature T = 300 K. The pure magnetite NPs have a saturation magnetization $M_{\text{sat}} = 24.2 \text{ A} \cdot \text{m}^2/\text{kg}$, and a magnetic mass susceptibility, the slope of the magnetization curve at $H \to 0$, of $\chi_{\text{mass}} = 1.6 \text{ cm}^3/\text{g}$. Consistent with the magnetic properties of ferromagnetic materials of just a few nanometers in size, the remnant magnetic moment is M_r < 0.3 A·m²/kg at zero magnetic field. There is no measurable hysteresis.

The magnetic properties for DB1/magnetite NPs that are coated at two different magnetite NP concentrations are also measured (see Methods for experimental details). For the lower concentration (0.4 wt % of magnetite NPs, which corresponds to approximately 3000 magnetite NPs per a dumbbell-shaped particles), the $M_{\rm sat}$ and $\chi_{\rm mass}$ values are 14.1 A·m²/kg and 0.81 cm³/g. For composite particles syn-

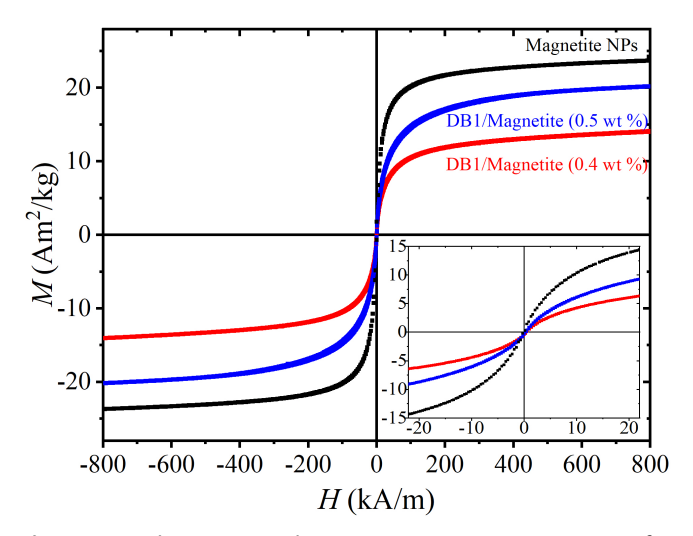


Figure 4: Vibrating sample magnetometer measurement of DB/magnetite multi-layered particles. Magnetization curves of pure magnetite nanoparticles (black), DB1/magnetite (0.5 wt %, blue), and DB1/magnetite (0.4 wt %, red) particles are presented as magnetic field, *H* versus magnetic moment, *M*. An inset at bottom right shows hysteresis loops from -24 to 24 kA/m, showing no remnant magnetization at zero magnetic field, as well as no hysteresis.

the sized with 0.5 wt % of suspended magnetite NPs (approximately 4000 magnetite NPs per a DB particle), both $M_{\rm sat}$ and $\chi_{\rm mass}$ increase to 20.2 A·m²/kg and 1.05 cm³/g. These results demonstrate that the magnetic response of the NPs can be tailored by varying the amount of magnetite NPs during the adsorption steps.

Comparing both results for different magnetic NP concentrations, both the saturation magnetization and the magnetic mass susceptibility increase with the amount ratio of magnetic to nonmagnetic material; increasing the magnetite NP concentration or decreasing nonmagnetic seed concentration in the composite particles increases both the saturation magnetization and the magnetic mass susceptibility.[39, 40] Because the magnetic properties can be tailored by varying the amount of magnetic NPs, this observation confirms that LbL adsorption method allows the fabricated magnetic NPs to be tuned for target magnetic properties.

The number density of adsorbed magnetite nanoparticles in the nonmagnetic/magnetic (DB/magnetite) composite particles can be estimated by the Langevin model[41, 42]

$$M = N m_{\rm np} \left[\coth \left(\frac{\mu_0 m_{\rm np} H}{k_{\rm B} T} \right) - \frac{k_{\rm B} T}{\mu_0 m_{\rm np} H} \right]$$
 (1)

where a product of magnetic particle number N and its moment $m_{\rm np}$ is the $M_{\rm sat},~\mu_0$ is the vacuum permeability, and $k_{\rm B}T$ is the Boltzmann energy at the absolute temperature T. The first order term of a Taylor expansion of equation 1 provides the magnetic susceptibility, $\chi = \mu_0 N m_{\rm np}^2/3k_{\rm B}T$. Given the magnetic moment of a magnetic NP $(m_{\rm np}^2)$, the magnetic mass susceptibility ratio of

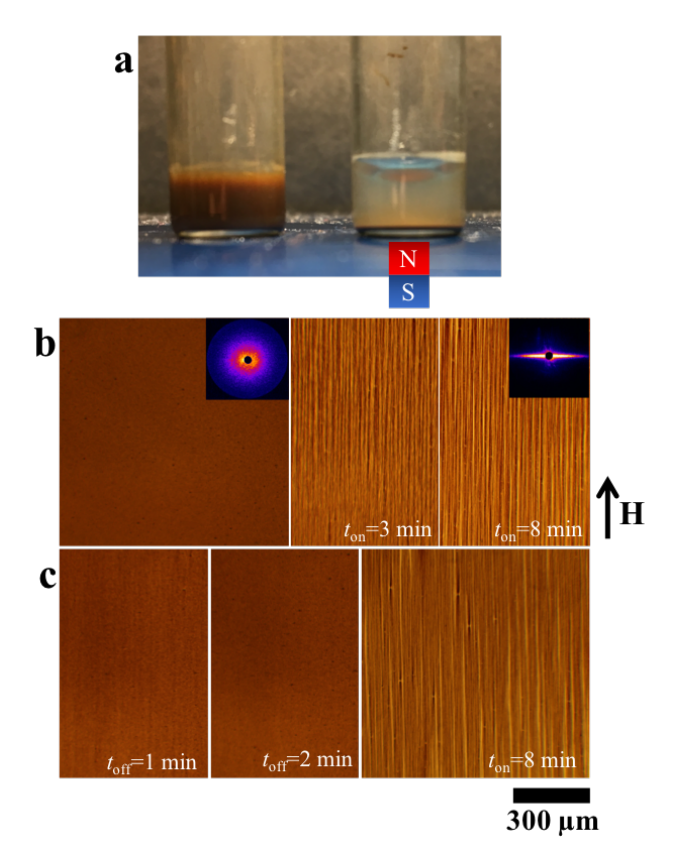


Figure 5: Magnetic response of the synthesized anisotropic nanoparticles. a An image of DB1/magnetite (0.5 wt %) suspension under no magnetic field (left) and with neodymium magnets at the bottom of the vial (right) show the macroscopic separation of magnetic particles. **b** Micrographs of DB1/magnetite particle suspension (0.5 vol %) show that particles are well-dispersed in the absence of a magnetic field (left panel) and form column-like microstructures under external magnetic field (1750 A/m). The microstructure grows as the field-applied time (t_{on}) increases (middle panel: $t_{on} = 3$ min; right panel: $t_{on} = 8 \text{ min}$). c The microstructures deform when the magnetic field is tuned off and particles redisperse. Left and middle panels show the deformation of the microstructures and particle redispersion after field-off time duration $t_{\rm off}=1$ min and $t_{\text{off}} = 2$ min, respectively. The suspended particles can again form column-like structures under the magnetic field. Insets are small-angle light scattering patterns under the corresponding conditions. An arrow indicates the direction of applied magnetic field.

magnetite NPs and DB/magnetite enables us to estimate the number of magnetite NPs coated on the dumbbell-shaped NPs. DB/magnetite particles fabricated with 0.4 wt % and 0.5 wt % magnetite NP concentration gives 2100 and 3600 magnetite NPs per a dumbbell particle, respectively. These values are comparable to the ratios of magnetic and polymer NPs used in during the synthesis and with the image analysis results. Moreover, by substituting the magnetic susceptibility term in the Langevin model, the magnetic properties of the synthesized superparamagnetic particles can be fitted as shown in Figure S2.

3.3. Response to an External Field

The composite particles disperse well in water (Figure 5a, left) and migrate towards a strong neodymium magnet (Figure 5a, right). In addition to this bulk macroscopic separation behavior, the superparamagnetic particles interact with each other in the presence of magnetic field to form column-like microstructures, similar to other superparamagnetic particles.[43, 44] We observe their assembly and disassembly when a field is applied, then removed. The particle suspension is placed in at the center of Helmholtz coils and imaged using an optical microscope. The DB1/magnetite NP suspension is stable and dispersed, as shown in Figure 5b (left panel) in the absence of a field. Under a magnetic field (H = 1750 A/m) they form column-like structures in a direction parallel to the applied field (middle and right panels in Figure 5b). The formation of macrostructures of magnetic NPs under magnetic fields are similar with early-stage column-like structures formation of ferrofluid droplets[43, 44] and columnar domain formation of magnetic latex spheres under toggled magnetic fields[14, 13, 45]. The insets of Figure 5b are small-angle light scattering patterns at the corresponding field condition, which has an isotropic pattern in the absence of a field, indicating an isotropic dispersion of the NPs, but a highly anisotropic one when the field is switched on.

Microscopy also shows that the particles readily redisperse when the magnetic field is removed or an induced field turned off. In Figure 5c, we show the relaxation of the column-like microstructure. When the field is turned off, the particles immediately diffuse and as field-off time duration increases, $t_{\rm off}=1$ min in the left panel and $t_{\rm off}=2$ min in the middle panel, the microstructures completely disappear. The redispersed particles can still assemble, as shown in the right panel of Figure 5c, and redisperse repeatedly. These assembly and disassembly processes are shown in Supplementary Movie 1.

3.4. Colloidal Stability

We estimate the colloidal stability of the synthesized particles based on their ability to aggregate in a magnetic field and redisperse when the field is removed. The maximum dipole interaction

$$U_{\text{max}} = -\frac{m^2}{2\pi\mu_0 r^3} \tag{2}$$

with the magnetic moment m, and center-to-center distance of dipoles r relative to the Brownian thermal energy $k_{\rm B}T$ is the dipole strength

$$\lambda \approx U_{\text{max}}/k_{\text{B}}T.$$
 (3)

For the dumbbell colloids, $m = V_{\rm DB} \mu_0 \chi H$ and $\lambda = V_{\rm DB}^2 \mu_0 \chi^2 H^2 / 2\pi r^3 k_{\rm B} T$. When the field is applied with strength H=1750 A/m, $\lambda\approx 9$, which is consistent with the observed assembly behavior. The repulsive electrostatic stability barrier must be at least as large to account for the particles' redispersion when the field is removed. Detailed

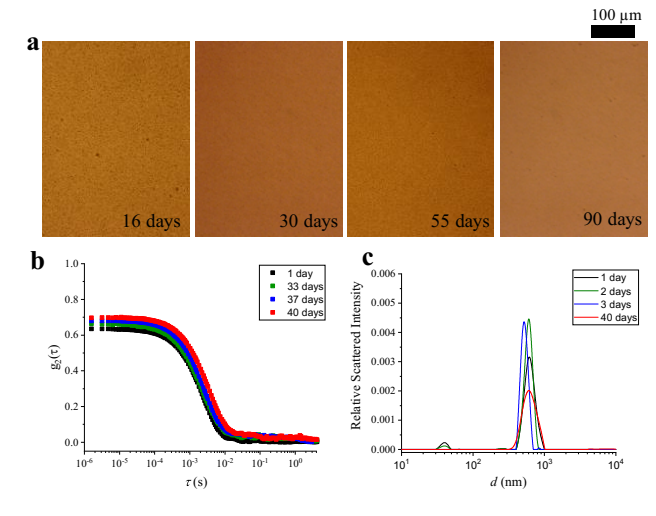


Figure 6: Long-term stability of the fabricated magnetic particle. **a** Micrographs of the DB1/magnetite suspension (0.5 vol %) show no significant aggregation behavior. **b** Autocorrelation functions for the short-period and long-period aged suspension are compared. **c** The size distributions of the particles at 1 (black), 2 (green), 3 (blue), and 40 (red) days are measured by the dynamic light scattering.

calculations of the interaction potential, including van der Waals, magnetic, and electrostatic double layer interactions with and without an applied field are presented in Supplemental Figures S3 and S4, respectively. The calculations support our observations of the suspension's colloidal stability and assembly. The induced attractive interaction is a secondary minimum in the interaction energy with respect to particle separation and a significant stability barrier exists and prevents particles from aggregating in the primary van der Waals minimum.

We monitored the colloidal stability of the dumbbell particles over a period of 90 days. Microscopy images (Figure 6a) show that the particles remain dispersed and that no aggregates form. Dynamic light scattering results (Figures 6b and c) also indicate good colloidal stability over long periods. The measured correlation functions are reproducible and the size distribution, calculated by a CONTIN method,[46] are consistent with the nominal diameter of 500nm.

4. Conclusion

We used an LbL method to fabricate magnetic responsive metal/polymer multi-layered nanoparticles with anisotropic shapes. Using the hydrophobic and electrostatic interactions between anisotropic PS colloids and charged polyelectrolytes or magnetite NPs, polymeric colloidal particles are coated by magnetite NPs. It was shown that the fabricated particles exhibit a magnetic response based on adsorbed magnetite NPs.

Two particle geometries (dumbbell-shaped and ellipsoidal PS particles with different aspect ratios) were examined to investigate the influence of particle shape and structure. Regardless the curvature of the seed nanoparticle, the synthesis yields particles with identical structures, demonstrating that a range of polymer colloid shapes are amenable to such methods; however, the synthesis of the ellipsoidal polymer colloids is currently limiting to the point that we do not have sufficient material for magnetometry, light scattering, or stability studies, which will have to be performed in the future. Nonetheless, we do note that they were colloidally stable when dispersed and responded to external magnetic fields identically to the other paramagnetic colloids.

Similar to the magnetic properties of the magnetite NPs, the magnetic dumbbell NPs were superparamagnetic. Furthermore, the magnetic moments were tunable by varying magnetite NP compositions; an increase in magnetic NPs resulted in higher saturation magnetization and magnetic susceptibility. Based on the magnetic moments, in the presence of external magnetic field the anisotropic magnetic particles formed column-like structures parallel to the direction of the magnetic field, whereas particles under no magnetic field remain well-dispersed.

This method is a comprehensive means to transform polymeric colloidal particles into magnetic NPs and can be used for many colloid shapes, structures, and chemical compositions, provided that there are sufficient hydrophobic and electrostatic interactions for the LbL deposition. In addition to the biomedical applications, it is of great interest to further study applications of the fabricated anisotropic colloids with magnetic response for investigating self-assembly behavior of non-spherical particles[3, 17] and as anisotropic microrheological probes, especially for non-linear microrheology.[47, 48, 49]

Acknowledgements

The authors thank Jee Young Lee and Keck CAMM (University of Delaware, Newark, DE) for the TEM imaging and P. J. Beltramo and J. Vermant for providing ellipsoidal nanoparticles. Funding from the NSF (CBET-1637991) is acknowledged.

References

- Ahmet Faik Demirörs, Diana Courty, Rafael Libanori, and André R. Studart. Periodically microstructured composite films made by electric- and magnetic-directed colloidal assembly. *Proceedings of the National Academy of Sciences*, 113(17):4623–4628, 2016.
- [2] Marek Grzelczak, Jan Vermant, Eric M. Furst, and Luis M. Liz-Marzán. Directed self-assembly of nanoparticles. ACS Nano, 4(7):3591–3605, 2010.
- [3] Tao Ding, Kai Song, Koen Clays, and Chen Ho Tung. Fabrication of 3D photonic crystals of ellipsoids: Convective self-assembly in magnetic field. Advanced Materials, 21(19):1936–1940, 2009.
- [4] Tao Ding, Kai Song, Koen Clays, and Chen Ho Tung. Controlled directionality of ellipsoids in monolayer and multilayer colloidal crystals. *Langmuir*, 26(13):11544–11549, 2010.
- [5] Wei Cheng, Jianjun Wang, Ulrich Jonas, George Fytas, and Nikolaos Stefanou. Observation and tuning of hypersonic bandgaps in colloidal crystals. *Nature materials*, 5(10):830–836, 2006.
- [6] Peter J. Beltramo, Dirk Schneider, George Fytas, and Eric M. Furst.

- Anisotropic hypersonic phonon propagation in films of aligned ellipsoids. *Physical Review Letters*, 113(20):1–5, 2014.
- [7] Jason D Forster, Jin-Gyu Park, Manish Mittal, Heeso Noh, Carl F Schreck, Corey S O'Hern, Hui Cao, Eric M Furst, and Eric R Dufresne. Assembly of Optical Scale Dumbbells Into Dense Photonic Crystals. ACS nano, (8):6695–6700, 2011.
- [8] Eric M. Furst. Directed self-assembly. Soft Matter, 9:9039–9045, 2013.
- [9] Fangfang Chu, Nils Heptner, Yan Lu, Miriam Siebenbürger, Peter Lindner, Joachim Dzubiella, and Matthias Ballauff. Colloidal plastic crystals in a shear field. *Langmuir*, 31(22):5992–6000, 2015.
- [10] R Pethig, Ying Huang, Xiao bo Wang, and J P H Burt. Positive and negative dielectrophoretic collection of colloidal particles using interdigitated castellated microelectrodes. *Journal of Physics D: Applied Physics*, 25(5):881, 1992.
- [11] V. G. Levich. Physicochemical hydrodynamics. Prentice-Hall Inc., 1962.
- [12] M. Trau, D. A. Saville, and I. A. Aksay. Assembly of Colloidal Crystals at Electrode Interfaces. *Langmuir*, 13(24):6375–6381, 1997.
- [13] James W. Swan, Paula A. Vasquez, Peggy A. Whitson, E. Michael Fincke, Koichi Wakata, Sandra H. Magnus, Frank De Winne, Michael R. Barratt, Juan H. Agui, Robert D. Green, Nancy R. Hall, Donna Y. Bohman, Charles T. Bunnell, Alice P. Gast, and Eric M. Furst. Multi-scale kinetics of a field-directed colloidal phase transition. *Proc. Nat. Acad. Sci.*, 109(40):16023–16028, 2012.
- [14] James W. Swan, Jonathan L. Bauer, Yifei Liu, and Eric M. Furst. Directed colloidal self-assembly in toggled magnetic fields. *Soft Matter*, 10(8):1102, 2014.
- [15] Jianping Ge, Yongxing Hu, Tierui Zhang, and Yadong Yin. Superparamagnetic composite colloids with anisotropic structures. *Journal* of the American Chemical Society, 129(29):8974–8975, 2007.
- [16] Bohdan Senyuk, Michael C. M. Varney, Javier A. Lopez, Sijia Wang, Ning Wu, and Ivan I. Smalyukh. Magnetically responsive gourdshaped colloidal particles in cholesteric liquid crystals. *Soft Matter*, 10:6014–6023, 2014.
- [17] Hojin Kim, Jonathan L Bauer, Paula A Vasquez, and Eric M Furst. Structural coarsening of magnetic ellipsoid particle suspensions driven in toggled fields. *Journal of Physics D: Applied Physics*, 52(18):184002, mar 2019.
- [18] Dhananjay Dendukuri, Kim Tsoi, T. Alan Hatton, and Patrick S. Doyle. Controlled synthesis of nonspherical microparticles using microfluidics. *Langmuir*, 21(6):2113–2116, 2005.
- [19] Dhananjay Dendukuri, Daniel C. Pregibon, Jesse Collins, T. Alan Hatton, and Patrick S. Doyle. Continuous-flow lithography for highthroughput microparticle synthesis. *Nature Materials*, 5:365–369, 04 2006.
- [20] Julie A. Champion, Yogesh K. Katare, and Samir Mitragotri. Particle shape: A new design parameter for micro- and nanoscale drug delivery carriers. *Journal of Controlled Release*, 121(1-2):3–9, 2007.
- [21] Julie A. Champion, Yogesh K. Katare, and Samir Mitragotri. Making polymeric micro- and nanoparticles of complex shapes. *Proceedings* of the National Academy of Sciences, 104(29):11901–11904, 2007.
- [22] Frank Caruso, Andrei S. Susha, Michael Giersig, and Helmuth Möhwald. Magnetic Core-Shell Particles: Preparation of Magnetite Multilayers on Polymer Latex Microspheres. Advanced Materials, 11, 1999.
- [23] Harpreet Singh, Paul E. Laibinis, and T. Alan Hatton. Rigid, superparamagnetic chains of permanently linked beads coated with magnetic nanoparticles. Synthesis and rotational dynamics under applied magnetic fields. *Langmuir*, 21(24):11500–11509, 2005.
- [24] Kisun Yoon, Daeyeon Lee, Woong Kim, and David A Weitz. Asymmetric functionalization of colloidal dimer particles with gold nanoparticles. *Chemical Communication*, 48:9056–9058, 2012.
- [25] Randall M Erb, Rafael Libanori, Nuria Rothfuchs, and André R Studart. Composites Reinforced in Three Dimensions by Using Low Magnetic Fields. Science, 335:199–204, 2012.
- [26] Miguel A. Correa-Duarte, Marek Grzelczak, Veronica Salgueiriño-Maceira, Michael Giersig, Luis M. Liz-Marzán, Michael Farle, Karl

- Sierazdki, and Rodolfo Diaz. Alignment of carbon nanotubes under low magnetic fields through attachment of magnetic nanoparticles. *Journal of Physical Chemistry B*, 109(41):19060–19063, 2005.
- [27] A. R. Goodall, M. C. Wilkinson, and J. Hearn. Mechanism of emulsion polymerization of styrene in soap-free systems. *Journal of Polymer Science: Polymer Chemistry Edition*, 15(9):2193–2218, 1977.
- [28] Tetsuya Yamamoto, Masaki Nakayama, Yoichi Kanda, and Ko Hi-gashitani. Growth mechanism of soap-free polymerization of styrene investigated by AFM. *Journal of Colloid and Interface Science*, 297(1):112–121, 2006.
- [29] N. A. Kotov. Layer-by-layer self-assembly: the contribution of hidrophobic interactions. *NanoStructured Materials*, 12:789–796, 1999.
- [30] Juhyun Park and Paula T. Hammond. Polyelectrolyte multilayer formation on neutral hydrophobic surfaces. *Macromolecules*, 38(25):10542–10550, 2005.
- [31] Jin-Gyu Park, Jason D Forster, and Eric R Dufresne. High-yield synthesis of monodisperse dumbbell-shaped polymer nanoparticles. *Journal of the American Chemical Society*, 132:5960–5961, 2010.
- [32] Y. Chonde and I. M. Krieger. Emulsion polymerization of styrene with ionic comonomer in the presence of methanol. *Journal of Applied Polymer Science*, 26(6):1819–1827, 1981.
- [33] C. C. Ho, A. Keller, J. A. Odell, and R. H. Ottewill. Preparation of monodisperse ellipsoidal polystyrene particles. *Colloid & Polymer Science*, 271(5):469–479, 1993.
- [34] K. M. Keville, E. I. Franses, and J. M. Caruthers. Preparation and characterization of monodisperse polymer microspheroids. *Journal* of Colloid And Interface Science, 144(1):103–126, 1991.
- [35] Gleb B. Sukhorukov, Edwin Donath, Heinz Lichtenfeld, Eberhard Knippel, Monika Knippel, Axel Budde, and Helmuth Möhwald. Layer-by-layer self assembly of polyelectrolytes on colloidal particles. Colloids and Surfaces A: Physicochemical and Engineering Aspects, 137(1):253 – 266, 1998.
- [36] Yudhisthira Sahoo, Alireza Goodarzi, Mark T. Swihart, Tymish Y. Ohulchanskyy, Navjot Kaur, Edward P. Furlani, and Paras N. Prasad. Aqueous Ferrofluid of Magnetite Nanoparticles: Fluorescence Labeling and Magnetophoretic Control. *Journal of physical Chemistry B*, 109:3879–3885, 2005.
- [37] Herbert A. Sturges. The choice of a class interval. *Journal of the American Statistical Association*, 21(153):65–66, 1926.
- [38] David Ková, Aneta Malá, Jitka Mlcochová, Michal Kalina, Zdenka Fohlerová, Antonín Hlaválek, Zdenek Farka, Petr Skládal, Zenon Starcuk Jr, Radovan Jirík, Ondrej Slabý, and Jaromír Hubálek. Preparation and characterisation of highly stable iron oxide nanoparticles for magnetic resonance imaging. *Journal of Nanomaterials*, 2017:1–9, 2017.
- [39] Hong Xu, Longlan Cui, Naihu Tong, and Hongchen Gu. Development of high magnetization Fe3O4/polystyrene/silica nanospheres via combined miniemulsion/emulsion polymerization. *Journal of the American Chemical Society*, 128(49):15582–15583, 2006.
- [40] Christy R. Vestal and Z. John Zhang. Atom transfer radical polymerization synthesis and magnetic characterization of MnFe2O4polystyrene core/shell nanoparticles. *Journal of the American Chemical Society*, 124(48):14312–14313, 2002.
- [41] Langevin, P. Sur la théorie du magnétisme. J. Phys. Theor. Appl., 4(1):678–693, 1905.
- [42] Alexey O. Ivanov, Sofia S. Kantorovich, Evgeniy N. Reznikov, Christian Holm, Alexander F. Pshenichnikov, Alexander V. Lebedev, Alexandros Chremos, and Philip J. Camp. Magnetic properties of polydisperse ferrofluids: A critical comparison between experiment, theory, and computer simulation. *Phys. Rev. E*, 75:061405, Jun 2007.
- [43] Joanne H E Promislow and Alice P Gast. Magnetorheological Fluid Structure in a Pulsed Magnetic Field. *Langmuir*, 12(14):4095–4102, 1996
- [44] J H E Promislow and A P Gast. Low-energy suspension structure of a magnetorheological fluid. *Physical Review E*, 56(1):642–651, 1997.
- [45] James W. Swan, Paula A. Vasquez, and Eric M. Furst. Buckling instability of self-assembled colloidal columns. *Physical Review Letters*,

Paramagnetic dumbbell and ellipsoid colloids

- 113(3):1-5, 2014.
- [46] Stephen W Provencher. CONTIN: A general purpose constrained regularization program for inverting noisy linear algebraic and integral equations. *Comput. Phys. Commun.*, 27:229, 1982.
- [47] E. M. Furst and T. M. Squires. *Microrheology*. Oxford University Press, New York, 2017.
- [48] Todd M Squires. Nonlinear microrheology: Bulk stresses versus direct interactions. *Langmuir*, 24:1147–1159, 2008.
- [49] Ryan J DePuit and Todd M Squires. Micro-macro discrepancies in nonlinear microrheology: II. Effect of probe shape. J. Phys. Condens. Matter, 24(46):464107, 2012.